COBEM 2023 27TH INTERNATIONAL CONGRESS OF MECHANICAL ENGENEERING

ABCM Brazilian Society of Mechanical Sciences and Engineering
27th ABCM International Congress of Mechanical Engineering
December 04-08, 2023, Florianópolis-SC, Brazil

COB-2023-1072
PRELIMINARY CONSTITUENT ANALYSIS FOR THE MANUFACTURE OF A COMPOSITE WITH ACTIVE POTENTIAL

João Pedro Rodrigues Deodato
Federal Rural University of the Semi-Arid Region - UFERSA, R. Francisco Mota, N° 572, Pres. Costa e Silva, Mossoró/ RN, CEP 59.625-900.
jpdeodato@ufc.br

Ramon Rudá Brito Medeiros
Federal University of Ceará - UFC, R. Felipe Santiago, N° 411, Cidade Universitária, Russas/CE, CEP 62.900-420.
ramon.ruda@ufc.br

Talita Rebouças de Araújo Cortez
Michelle de Queiroz Nunes
Zoroastro Torres Vilar
Rodrigo Nogueira de Codes
Federal Rural University of the Semi-Arid Region - UFERSA, R. Francisco Mota, N° 572, Pres. Costa e Silva, Mossoró/ RN, CEP 59.625-900.
talitararaujo@outlook.com, michellequeiroz03@gmail.com, zoroastro@ufersa.edu.br, rncodes@ufersa.edu.br

Abstract. *Smart materials have the ability to adapt to changes in the environment they are placed in by altering their properties under specific operational circumstances. These properties enable applications in compact, powerful, and lightweight thermomechanical actuators for various sectors. In this study, a glass fiber-reinforced polymer (GFRP) was manufactured and characterized, along with the thermomechanical characterization of wires made of a Ni-Ti shape memory alloy (SMA), which were incorporated into the matrix to produce an active composite. The study includes the investigation and characterization of the constituents, such as thermal analysis of the resin synthesis using the thermogravimetric technique (TG). The Ni-Ti wire was characterized using the resistance-temperature test (RET), allowing for the determination of the resin's thermal deflection temperature (HDT) and the phase transformation temperatures of the Ni-Ti wire. Mechanical characterization of the components involved tensile tests on the wire, resin, and composites, aided by digital image correlation (DIC) technique to obtain information on deformation, elastic modulus behavior, and tensile strength of all components. The results confirmed that the resin's thermal deflection temperature and the phase transformation temperatures of the Ni-Ti wire allow for its incorporation into the composite, enabling the construction of a composite that has the capability to transfer load between the Ni-Ti wires and the GFRP.*

Keywords: *Composite, Digital Image Correlation (DIC), Characterization, Shape Memory Alloy, Thermomechanical analysis*

1. INTRODUCTION

In recent years, advancements in the field of smart materials and structures have generated significant interest within the science and materials engineering community. Smart materials constitute a special class of materials in which one or more properties can be modified and respond in a predetermined manner to environmental stimuli (Wieszczycka *et al.*, 2021; Tani *et al.*, 1998; Lendlein *et al.*, 2018). These materials are sensitive to external stimuli such as temperature, stress, light, humidity, as well as electric and magnetic fields, and they react to such stimuli by changing their properties (mechanical, electrical, or visual), structure, or functions (Smith and Hashemi, 2012; Jain *et al.*, 2023). Smart materials find diverse applications across various sectors, including healthcare, aerospace, civil infrastructure, and the environment. Due to their responsiveness to the external environment, these materials possess an embedded sensor, an actuator, and a control mechanism that assist them in responding to the environment (Shukla and Garg, 2023)..

Some smart materials developed so far include piezoelectric ceramics, piezoelectric polymers, electrorheological fluids, magnetic fluids, shape memory alloys, shape memory polymers, covalent adaptive network polymers, and electroactive polymers (Kim *et al.*, 2016; Savi and Oliveira, 2013). Among these materials, Shape Memory Alloys (SMAs) stand out, which are metals capable of returning to their original shape after being subjected to plastic deformation. Shape memory alloys (SMAs) have the ability to change from one crystalline structure to another in response to a stimulus in the form of temperature or stress. This change in structure means that the material has a specific shape at one tempera-

ture or stress level and an alternative shape at another. The two crystalline structures of SMAs are the low-temperature martensite phase and the high-temperature austenite phase (also known as the beta phase) (Arun *et al.*, 2018). Additionally, under specific conditions, SMAs can absorb and dissipate mechanical energy by undergoing a reversible hysteresis shape change when subjected to applied cyclic mechanical loads. These unique characteristics of SMAs have made them popular for applications such as sensing and actuation, impact absorption, and vibration damping (Lagoudas, 2008; Yang, 2000; Sacco and Artioli, 2015).

The ability of SMAs to return to a predetermined shape upon heating is referred to as the shape memory effect (SME), while the ability to recover large deformations (approximately ($\approx 8\%$)) and exhibit significant stress-strain hysteresis associated with mechanical loading-unloading under isothermal conditions is known as superelasticity/pseudoelasticity (SE) (Rao *et al.*, 2015; Zhang *et al.*, 2020). SMAs of the NiTi system, also known as Nitinol, are renowned for their excellent combination of functional properties, incorporating the thermomechanical phenomena of shape memory effect and superelasticity. These characteristics enable a wide range of applications in industries such as aerospace, automotive, mechatronics, medical devices, and dentistry (Amorim *et al.*, 2015). The incorporation of SMA wires or particles into a desired polymeric matrix allows the development of active composites. This category of materials offers a broad range of opportunities and promotes technological innovation by meeting the demand for stronger, lighter, more versatile, and, above all, functional materials (Leal *et al.*, 2012).

To measure deformation and failure behavior in composite materials, digital image correlation (DIC) is increasingly being used as a non-contact optical technique for deformation and displacement measurements (Lindström *et al.*, 2023). The heterogeneous nature of the composite microstructure results in complex local behavior that cannot be adequately captured through traditional experimental characterization techniques. The application of DIC offers significant advantages in monitoring this behavior, especially for fiber-reinforced composite materials (Holmes *et al.*, 2023).

This article presents an experimental analysis of the mechanical behavior of glass fiber-reinforced polymer (GFRP) and a Ni-Ti wire, which are candidates for components of an active composite. Tensile tests were performed on the wire, the resin, and the composites for the mechanical characterization of the components, aided by the digital image correlation (DIC) technique, which was used to obtain information on the deformation, modulus of elasticity behavior, and tensile strength limit of all the components. The activation potential of the Ni-Ti wire was also obtained through tensile testing at different temperatures. The results enable the design of a composite material with the ability to transfer and measure the load between the Ni-Ti wires and the GFRP.

2. MATERIALS AND METHODS

2.1 Composite lamination and choice of activator

For the development of the current study, a laminate composed of epoxy matrix with a glass fiber fabric with six layers was fabricated, with each layer arranged in the same orientation. The polymeric matrix consists of the SQ 2001 resin system and the SQ 3154 hardener. According to the manufacturer, this combination is suitable for fiberglass, carbon, and aramid (Kevlar) laminates, cured at room temperature. For structural reinforcement, a bi-directional fabric with a 3 x 1 twill weave of E-glass fiber was used, commercially designated as AF-0201, with a grammage of 200 $\pm$ 20 g/m² and a thickness of 0.20 $\pm$ 0.3 mm.

The glass fiber laminate was produced using the hand lay-up method. The lamination of the composites was carried out on a 10 mm thick glass sheet, using a mold release agent based on carnauba wax called TR Mold Release. The process of impregnating the fabrics was done layer by layer with resin, using a brush and roller to remove excess resin.

The selected wires as the activating element are equiatomic NiTi (nickel-titanium) superelastic wires with a diameter of 0.6 mm and a polished surface, provided by Magerial Science company.

2.2 Specimens and configurations

To obtain the samples of the laminate, a circular saw was used, utilizing the IRWIN segmented diamond blade with a diameter of ⌀4 - 3/8" x 3/4" (110 mm x 20 mm). Subsequently, the samples were sanded and polished to achieve the required finish and dimensional tolerance.

For the fabrication of the cured resin samples, the resin/hardener mixture was poured into a printed PLA (polylactic acid) mold, which was positioned between two glass sheets coated with a mold release agent.

Finally, for the use of the digital image correlation (DIC) technique, the test specimens were painted with black spray paint and sprayed with white droplets, creating a gray pattern texture on their surface. For the tensile and electrical resistance tests on the NiTi wires, samples of approximately 200 mm and 50 mm in length, respectively, were extracted.

The test specimens for the uniaxial tensile tests on the laminate, cured resin, and NiTi wire followed the guidelines of ASTM standards D3039/D3039M (ASTM International, 2017), D638-22 (ASTM International, 2022), and E8/E8M (ASTM International, 2021), respectively. The geometry and dimensions of the test specimens are illustrated in Figure 1.

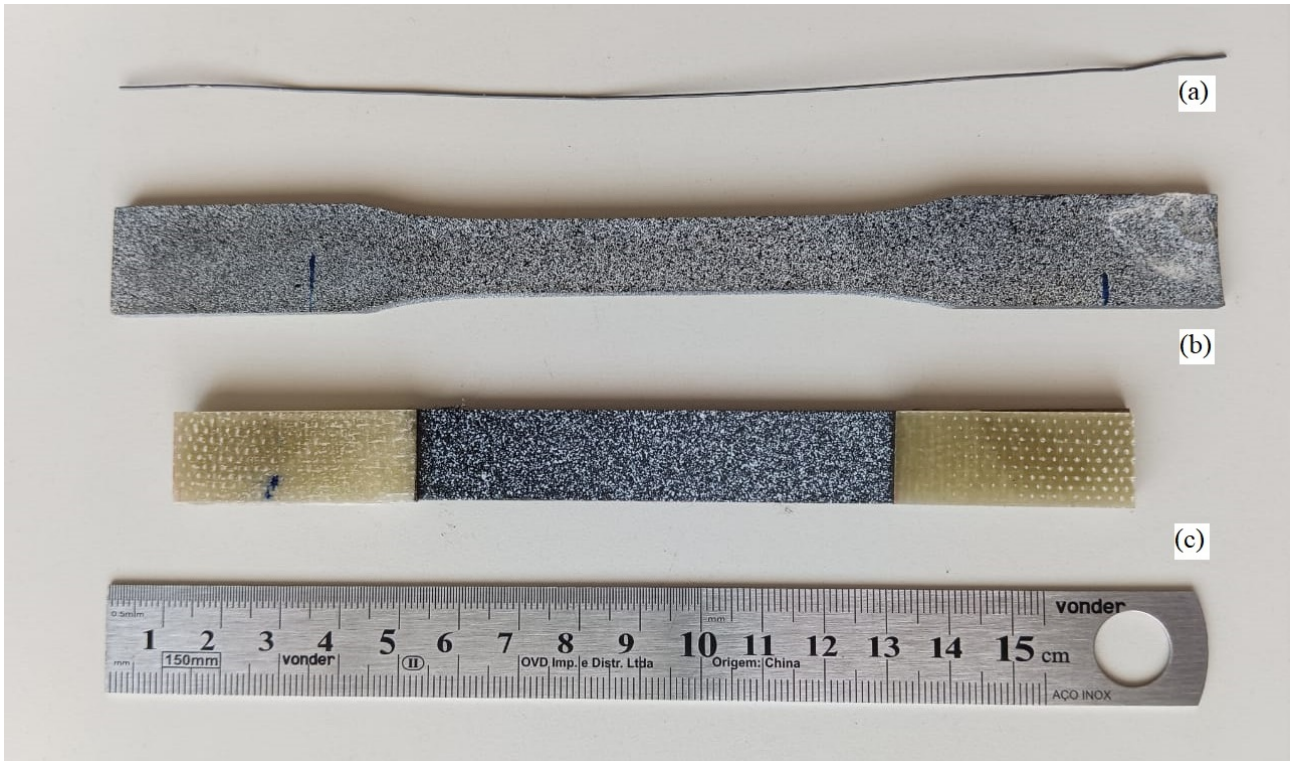

Figure 1. Geometry and dimensions of the test specimens: (a) Uniaxial tensile test of NiTi wire; (b) Uniaxial tensile test of resin; (c) Uniaxial tensile test of GPRF

2.3 Thermogravimetry (TGA)

Thermogravimetry (TGA) is a thermal analysis technique that focuses on measuring the mass variation of a material as its temperature is changed over time. This technique is widely used to investigate the degradation kinetics of materials.

The equipment used for the tests was the TGA Q50 TA Instruments, operated in a synthetic air atmosphere with a flow rate of 40 mL/min and a heating rate of 10°C/min in the temperature range of 25 to 900ºC. The epoxy resin samples were cut to a mass of approximately 25 mg.

2.4 Uniaxial Tensile Test

The uniaxial tensile tests were performed according to the ASTM standards D3039/D3039M (2017), D638-22 (2022), and E8/E8M (2021). The tests were conducted using an EMIC DL10000 universal testing machine with load cells of 30 kN and 5 kN, and a test speed of 0,008 mm/s. Strain measurements of the samples were performed using the digital image correlation (DIC) technique, using a CANON D60i digital camera with a 100 mm macro lens, acquiring an image every 5 seconds.

The uniaxial tensile tests on the wires were conducted according to the ASTM E8/E8M-22 standard at room temperature (21°C), using a 5 kN load cell, without atmosphere control. Due to the relatively small diameter of the wire, mandrels with sizes ranging from 1,5 to 10,0 mm and 3/8 - 24 UNF threads were used to fix the wire in the universal testing machine. Figure 2 presents the structure of the experimental setup for conducting the tests on all components.

The processing of the images obtained in the tests was performed using the open-source software NCORR V1.2, which is a 2D digital image correlation program. From the tests, it was possible to determine the following mechanical properties of the material: tensile strength (σ_R), longitudinal elastic modulus (E_y), and rupture strain (l_{rup}). Additionally, the software allowed for the determination of the strain distribution field across the cross-section of the materials.

2.5 Electrical Resistance Test

To analyze the variation of the material's electrical resistance as phase transformations occur, the wires were initially joined to four electrodes using resistance welding performed with a KERNIT micro-welder, model SMP 3000 GOLD. Through 0.30 mm flexible cables, the end electrodes were connected to a Keysight E3633A power supply that provided a constant current of 0.4A throughout the process. The remaining electrodes were connected to a data acquisition system, Keysight 34970A, which, along with a thermocouple, obtained the variation of electrical resistance with temperature.

The wires were submerged in a liquid medium and heated to the initial temperature of 100°C to initiate the mea-

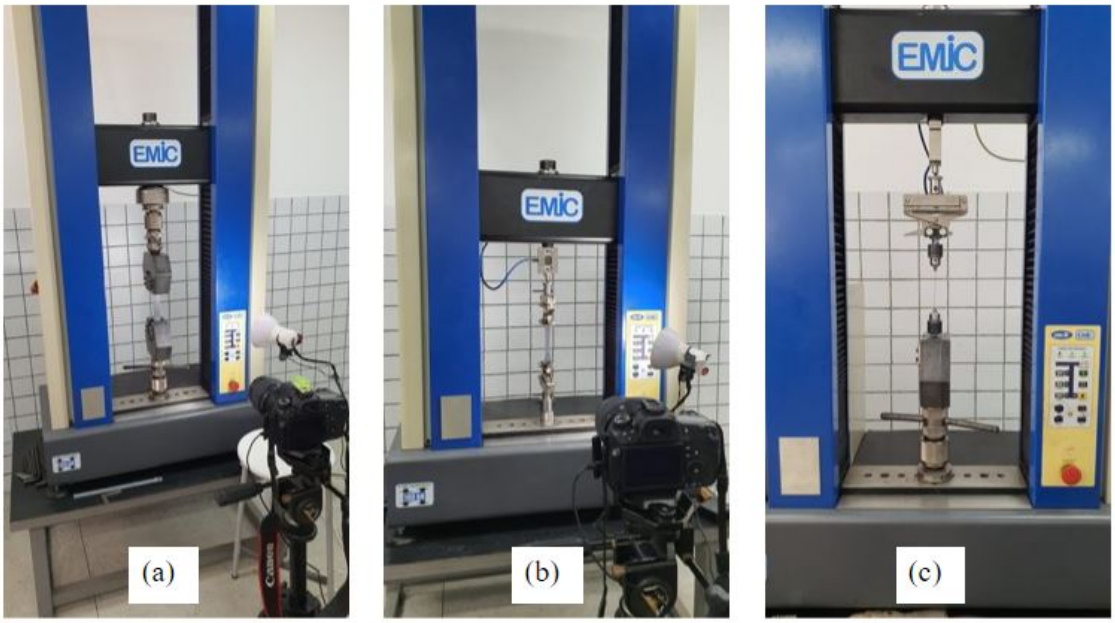

Figure 2. Experimental setup of the tensile test: (a)For the GPRF; (b) For the resin; (c) for the wire NiTi

surements. Once this temperature was reached, the sample was then cooled to 2°C and heated again to 100°C using a Novatecnica N1040 ultra-thermostatic bath. The structure of the experimental setup is illustrated in Figure 3.

Figure 3. Adjustable thermal bath system

3. RESULTS AND DISCUSSION

3.1 Thermogravimetry of cured resin

In Figure 4, the thermogravimetric analysis (TGA) result of the cured resin is presented, shown as the green curve. Three main events can be identified, with the second event being the most significant. The first event corresponds to a mass loss of 16,22%, occurring approximately between temperatures of 100ºC and 330ºC, attributed to the loss of volatile substances. The second event represents the temperature range where the major degradation of the resin occurred, accounting for approximately 57,59% of mass loss between 340ºC and 520ºC. The third event occurs within the temperature range of 530ºC to 630ºC, continuing the degradation of the resin until reaching a residual value of 0,10%. The derivative curve peaks indicate that the second and third events have maximum intensity at temperatures of 357,34ºC and 568,45ºC, respectively.

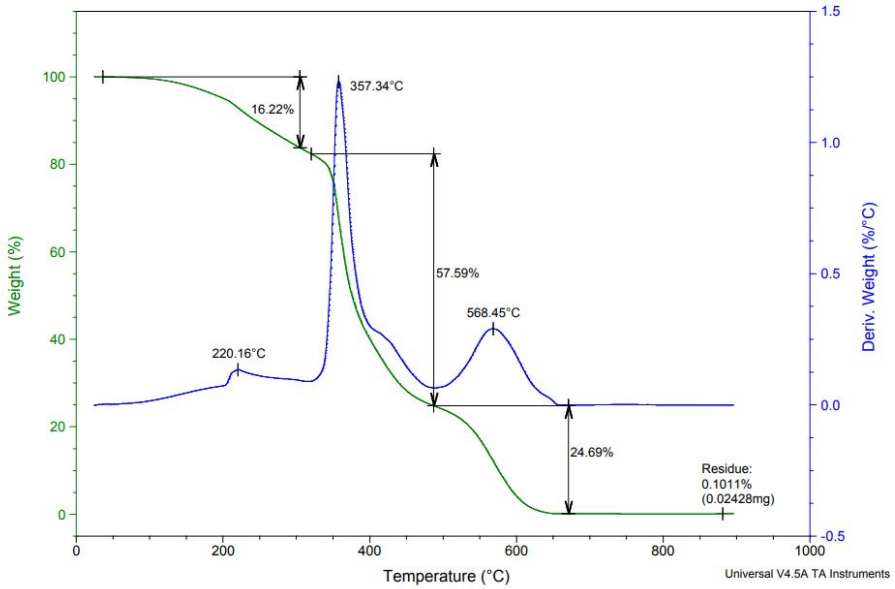

Figure 4. Thermogravimetry of cured resin

3.2 Tensile Test of Cured Resin

The results obtained through digital image correlation for the fourth sample of the resin are shown in Figure 5, and similar results were obtained for the other tests. In this analysis, it is worth noting that the presented result corresponds to the comparison between the reference image (first image) and the last image of the test.

In Figure 5 (a), we can see the vertical displacement experienced throughout the region of interest in the sample. It is possible to observe a sudden variation in the displacement zones as we approach the center of the sample, represented by more intense colors, indicating that the deformation in this direction is considerably greater in the region where fracture occurred. The material exhibits a similar behavior when analyzing the horizontal displacement, as observed in Figure 5 (b). Figure 5 (c) provides clearer evidence of the deformation concentration in the fracture region.

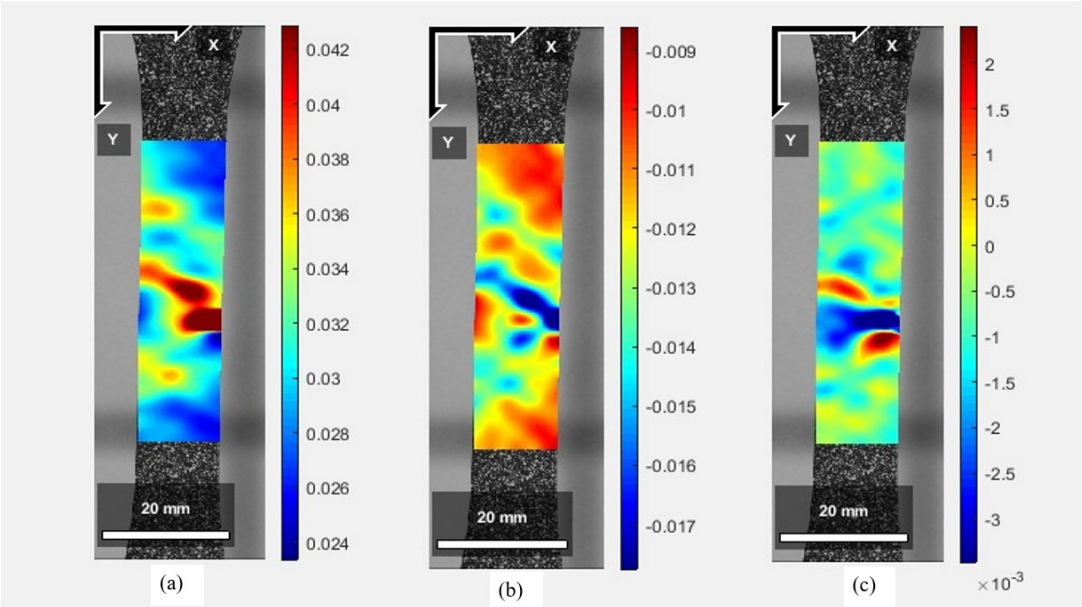

Figure 5. Digital image correlation for the resin.

Table 1 shows the results of the tests on the five resin samples, obtaining a tensile strength of 47,09 ± 3,41 MPa, a maximum strain of 0,029 ± 0,007, and an elastic modulus of 2,79 ± 0,05 GPa. Other researchers, such as Mesquita

(2018) and Mendonça (2019), have also reported similar values.

Table 1. Experimental results obtained for the properties of the resin

CPs	E_y (GPa)	σ_R (MPa)	l_{rup} (mm/mm)
CP01	2,82	48,83	0,0317
CP02	2,75	41,05	0,0197
CP03	2,80	47,87	0,0371
CP04	2,74	48,40	0,0237
CP05	2,85	49,27	0,0325
Average	2,79	47,09	0,0290
Standard deviation	0,05	3,41	0,0070
Standard deviation (%)	1,63%	7,25%	24,34%

Figure 6 shows the stress-strain curve of sample 2 of the resin. The other samples exhibited a similar behavior. From the graph, it can be observed that the resin demonstrated nearly elastic behavior throughout the entire test. No necking occurred in any of the samples, and failure occurred abruptly.

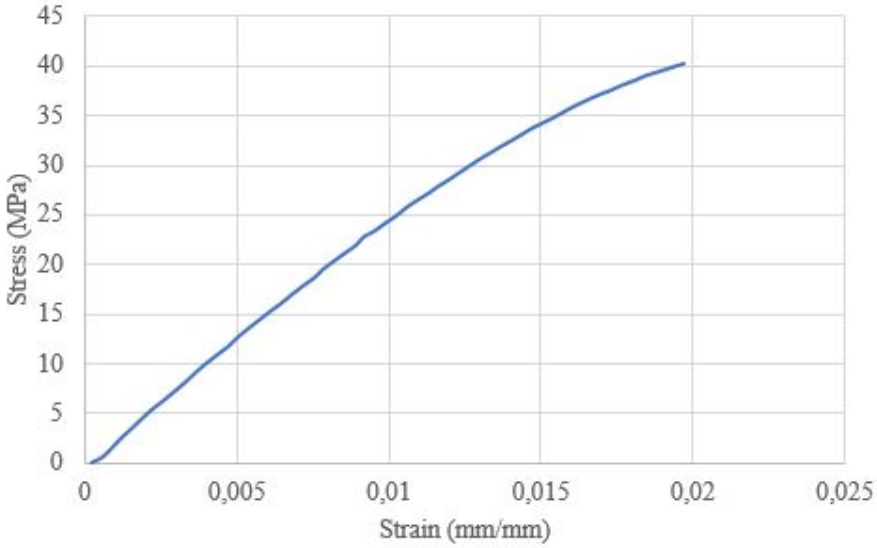

Figure 6. Stress x strain diagram for epoxy resin.

3.3 Tensile Test of GFRP

Figure 7 displays the results obtained through digital image correlation for the fourth sample of GFRP, with corresponding results observed for the other composite samples.

The behavior of the composite differs from that of the resin. In Figure 7 (a), the vertical displacement experienced throughout the region of interest in the sample is depicted. It can be observed that there is non-uniformity in the deformation, with higher deformation gradients found in the left region of the test specimen. Regarding the horizontal displacement, Figure 7 (b) shows that the highest deformation gradients are located in the lower-right region of the specimen. Figure 7 (c) reveals that, in general, the deformation is nearly uniform throughout most of the specimen, but there is a concentration of deformation as it approaches the fracture region in the upper part of the specimen.

Furthermore, in Figure 7 (b), narrow regions with higher levels of deformation can be observed diagonally along the entire specimen. These regions are attributed to the weave pattern of the fabric used as reinforcement, as they correspond to areas where fabric fibers overlap. Due to the twill weave structure of the fabric, these regions assume a diagonal configuration.

I have translated the text and provided the description of the figure. If you have any further text or specific requests, please let me know.

Analyzing the results from Table 2, it can be observed that the addition of the fabric resulted in an increase in the tensile strength and elastic modulus compared to the pure resin, with an average value of 202,76 $\pm$ 7,93 MPa for the maximum stress and 11,44 $\pm$ 0,40 GPa for the elastic modulus. However, there was a decrease in the maximum strain value, approximately 30%. Similar results can be found in studies conducted by Castro *et al.* (2000) and Silva (2011).

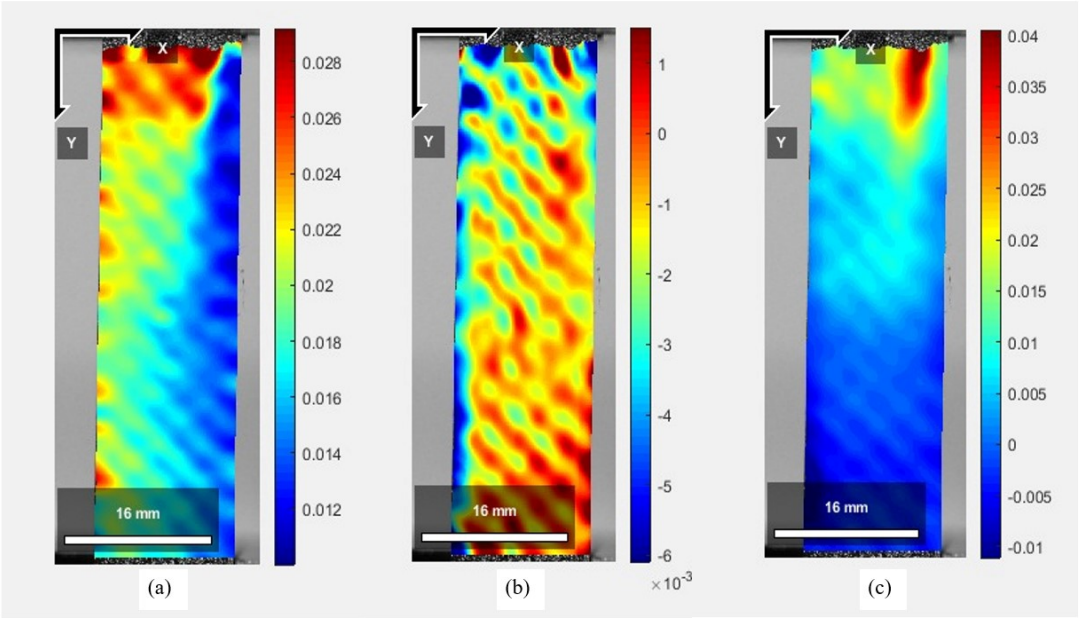

Figure 7. Digital Image Correlation for GFRP

Table 2. Experimental results properties of GRPF

CPs	E_y (GPa)	σ_R (MPa)	l_{rup} (mm/mm)
CP01	11,00	207,72	0,0181
CP02	12,07	194,16	0,0203
CP03	11,28	203,21	0,0214
CP04	11,50	195,76	0,0200
CP05	11,35	212,96	0,0214
Average	11,44	202,76	0,0202
Standard deviation	0,40	7,93	0,0014
Standard deviation (%)	3,46%	3,91%	6,79%

Figure 8 illustrates the stress-strain diagram for the fourth test conducted on GFRP specimens. Through the diagram, it is also evident that the use of fiberglass fabric as reinforcement increased the tensile strength and reduced the maximum strain of the sample. Additionally, it can be observed that the composite exhibited an elastic behavior until failure, with no necking formation in any of the samples and failure occurring abruptly.

3.4 Tensile test on NiTi wire

The curve shown in Figure 9 represents the test conducted on the second sample of the NiTi wire at a temperature of approximately 21°C. The tests for the other samples followed a similar procedure. According to the information obtained from the electrical resistivity test, the phase is primarily austenitic at point A with the presence of martensite phase. During the test, the applied stress only causes elastic deformation in the austenite phase, as shown by the A-B segment. Stress-induced martensite transformation (SIMT) begins nucleating at point B (100 MPa). It can be observed that as the elongation progresses, the volume fraction of martensite increases under approximately constant stress (B-C plateau). In this range, it is likely that both phases coexist, and there is a rearrangement of the martensite variants. Upon reaching point C, there is an increase in deformation due to an increase in stress. At point D, the stress level is sufficient to initiate plastic deformation of martensite, at around 960 MPa. Beyond this point, at a stress of approximately 1000 MPa, a region with a relatively small slope in the curve is observed, indicating the initiation of necking. Continuing with deformation until failure of the specimen, the high elasticity of the as-received wire is confirmed due to the exhibited strain rate, which approaches 40%.

Table 3 presents the values of yield strength (σ_E), elastic modulus for the austenite phase (E_A), tensile strength (σ_R), and maximum strain (l_{rup}) of the wire samples. The values of 38,93 $\pm$ 1,07 GPa for the elastic modulus and 0,41 $\pm$ 0,05 mm/mm for strain are acceptable when compared to those found in (Lagoudas, 2008) and (Sun *et al.*, 2017).

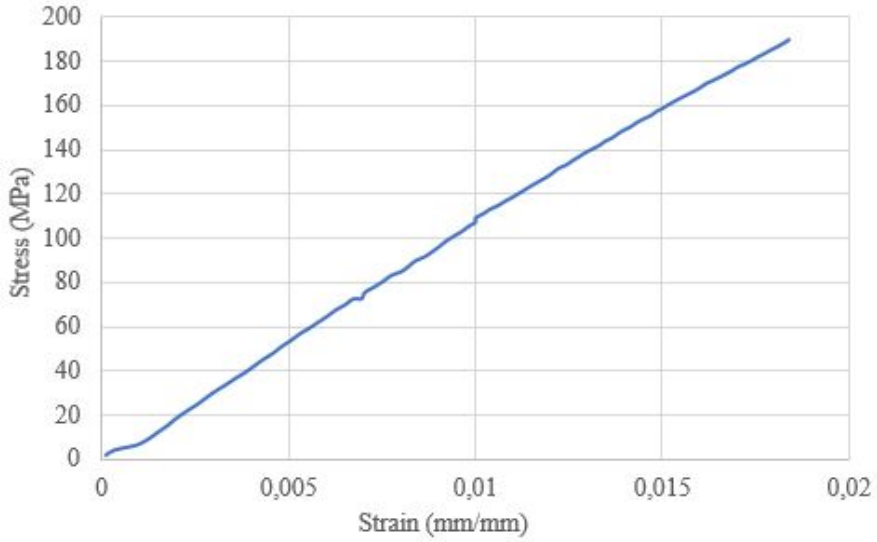

Figure 8. Stress x strain diagram for GPRF.

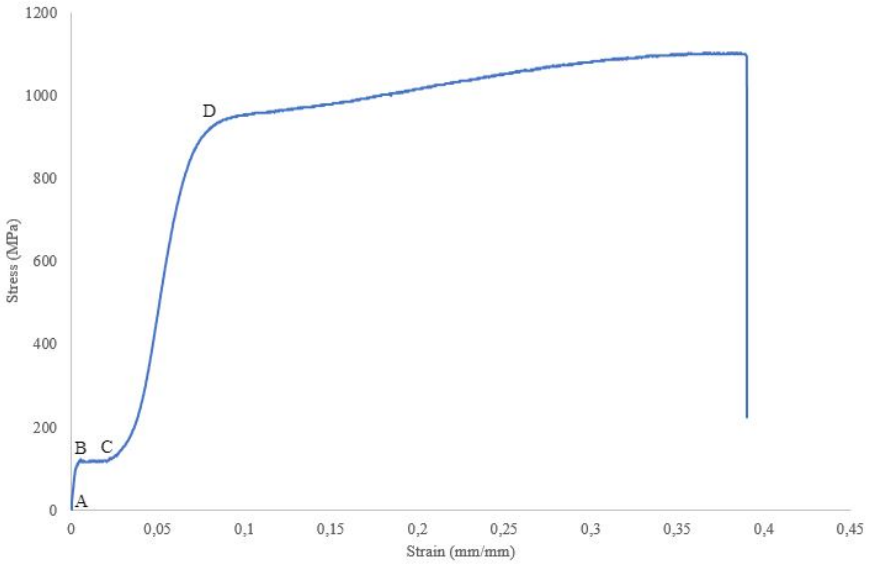

Figure 9. Stress x strain diagram for NiTi Wire.

Table 3. Experimental results properties of Fios NiTi

Sample	E_A **(Gpa)**	σ_E **(MPa)**	σ_R **(Mpa)**	l_{rup} **(mm/mm)**
AF01	37,78	103,99	1090,92	0,4650
AF02	39,13	103,41	1102,70	0,3901
AF03	39,89	102,58	1143,08	0,3709
Average	38,93	103,33	1112,23	0,41
Standard deviation	1,07	0,71	27,36	0,05
Standard deviation (%)	2,75%	0,69%	2,46%	12,17%

3.5 Electrical Resistance x Temperature Test

In the graphs obtained from the Electrical Resistance vs. Temperature (RET) tests, represented by the result of sample one in Figure 10, it is possible to observe the transformations from the martensite phase to austenite phase during heating and from austenite to martensite during cooling. In the figure, A_i represents the initial temperature of austenite formation, A_f the final temperature of the transformation to austenite, M_i the initial temperature of martensite formation, and M_f the final temperature of the transformation to martensite. By the tangent method, it can be inferred that the transformation

temperatures are approximately: $A_i = 17{,}3°C$, $A_f = 21{,}2°C$, $M_i = 16{,}1°C$, and $M_f = 20{,}0°C$. Similar results were obtained for the other samples.

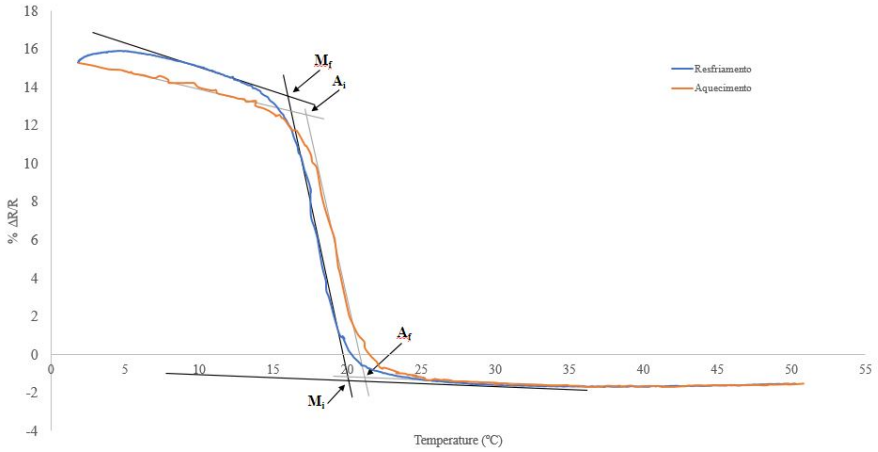

Figure 10. Electrical Resistance x Temperature Test for NiTi Wire.

4. CONCLUSIONS

The proposed manufacturing method for GFRP composite samples is capable of producing materials with good mechanical properties using limited resources, ensuring a controlled fabrication process to prevent material failures. Through RET and Thermogravimetry tests, it was found that the phase transformation temperatures of the NiTi wire are well below the resin's thermal deflection temperature, allowing the shape memory effect to be activated while the wires are embedded in the composite. This temperature difference would also enable an increase in the phase transformation temperatures through a heat treatment. It is believed that due to the high wettability of the NiTi wires and the strong adhesiveness of the epoxy resin, changes in the properties of the wires can be detected by digital image correlation.

Regarding the mechanical properties of the components, the obtained data allows for the calculation, using the rule of mixtures, of the fraction of NiTi wire that should be used for a specific project. Due to the high tensile strength and elasticity modulus of the wires compared to those of GFRP, even a small amount of the wires would cause a noticeable change in the properties of the final composite. The results obtained through digital image correlation were found to be quite satisfactory and efficient, providing the necessary properties for the realization of the active composite project.

5. REFERENCES

Amorim, F.A., Rodrigues, L.F.A., Araújo, C.J.d. and Maciel, T.M., 2015. "Avaliação das propriedades termomecânicas de fios de liga com memória de forma NiTi soldados por pulsos de micro TIG". *Soldagem Inspecão*, Vol. 20, No. 4, pp. 423–433.

Arun, D.I., Chakravarthy, P., R, A.K. and Santhosh, B., 2018. *Shape Memory Materials*. CRC Press, Boca Raton, FL.

ASTM International, 2017. *ASTM D3039/D3039M-17, Standard Test Method for Tensile Properties of Polymer Matrix Composite Materials*. West Conshohocken, PA.

ASTM International, 2021. *ASTM ASTM E8/E8M-22, Standard Test Methods for Tension Testing of Metallic Materials*. West Conshohocken, PA.

ASTM International, 2022. *ASTM D638-22, Standard Test Method for Tensile Properties of Plastics*. West Conshohocken, PA.

Castro, J.P., Daldosso, C.C., Shigue, C.Y. and Baldan†, C.A., 2000. "Estudo de propriedades mecânicas de compósitos epóxi/fibra de vidro para aplicação em temperaturas criogênicas". In *14°. CBECIMAT - Congresso Brasileiro de Engenharia e Ciência dos Materiais*. São Pedro – SP.

Holmes, J., Sommacal, S., Das, R., Stachurski, Z. and Compston, P., 2023. "Digital image and volume correlation for deformation and damage characterisation of fibre-reinforced composites: A review". *Compos. Struct.*, Vol. 315, No. 116994, p. 116994.

Jain, N., Nandu Ovhal, S., Patil, V. and Nani Kartik, K., 2023. "Smart materials - a state-of-the-art-review". *Mater. Today*.

Kim, H.C., Mun, S., Ko, H.U., Zhai, L., Kafy, A. and Kim, J., 2016. "Renewable smart materials". *Smart Mater. Struct.*, Vol. 25, No. 7, p. 073001.

Lagoudas, D.C., 2008. *Shape Memory Alloys*. Springer. ISBN 9780387476841.

Leal, A.S.C., Silva, S.M.L. and Araújo, C.J.d., 2012. "Comportamento termomecânico de compósitos ativos preparados com nanocompósitos epóxi/argila organofílica e fios de liga Ni-Ti com memória de forma". *Polímeros*, Vol. 22, No. 2, pp. 134–141.

Lendlein, A., Feng, Y., Grijpma, D.W. and Zhao, Y., 2018. "Smart materials". *ChemPhysChem*, Vol. 19, No. 16, pp. 1938–1940. ISSN 14397641. doi:10.1002/cphc.201800578.

Lindström, S.B., Wemming, H., Kapidžić, Z., Loukil, M.S. and Segersäll, M., 2023. "Integrated digital image correlation for mechanical characterization of carbon fiber-reinforced polymer plates". *Compos. Struct.*, Vol. 305, No. 116501, p. 116501.

Mendonça, V.C.d.S.M., 2019. *Caracterização das propriedades mecânicas de uma resina epoxy reforçada com nanotubos de carbono e ferro*. Mestrado em engenharia mecânica – produção industrial, Instituto Politécnico de Leiria, Lisboa.

Mesquita, P.H.X.d., 2018. *Caracterização Mecânica De Compósitos De Matriz Epóxi Reforçado Com Fibras De Sisal Em Diferentes Orientações Com Auxílio Da Correlação Digital De Imagens*. Programa de pós-graduação em ciência e engenharia de materiais, Universidade Federal Rural do Semi-Árido, Mossoró - RN.

Rao, A., Srinivasa, A.R. and Reddy, J.N., 2015. *Design of Shape Memory Alloy (SMA) Actuators*. Springer. ISBN 9783319031880.

Sacco, E. and Artioli, E., 2015. "SMA constitutive modeling and analysis of plates and composite laminates". In *Shape Memory Alloy Engineering*, Elsevier, pp. 141–192.

Savi, M. and Oliveira, S., 2013. "Os materiais inteligentes e suas aplicações". *Revista Marítima Brasileira*, Vol. v.133, pp. 39–56.

Shukla, U. and Garg, K., 2023. "Journey of smart material from composite to shape memory alloy (SMA), characterization and their applications-a review". *Smart Mater. Med.*, Vol. 4, pp. 227–242.

Silva, L.V.d., 2011. *Compósitos Avançados Epóxi/Fibra De Vidro com Elevado Teor de Nanotubos de Carbono*. Programa de pós-graduação em engenharia de minas, Universidade Federal do Rio Grande do Sul, Porto Alegre - RS.

Smith, W.F. and Hashemi, J., 2012. *Foundations of Materials Science and Engineering*. AMGH Editora Ltda., 5th edition. ISBN 9780073529240.

Sun, Q.P., Matsui, R., Takeda, K. and Pieczyska, E.A., eds., 2017. *Advances in shape memory materials*. Advanced structured materials. Springer International Publishing, Cham, Switzerland, 1st edition.

Tani, J., Takagi, T. and Qiu, J., 1998. "Intelligent material systems: Application of functional materials". *Appl. Mech. Rev.*, Vol. 51, No. 8, pp. 505–521.

Wieszczycka, K., Staszak, K., Woźniak-Budych, M.J., Litowczenko, J., Maciejewska, B.M. and Jurga, S., 2021. "Surface functionalization - the way for advanced applications of smart materials". *Coord. Chem. Rev.*, Vol. 436, No. 213846, p. 213846.

Yang, D., 2000. "Shape memory alloy and smart hybrid composites - advanced materials for the 21st century". *Mater. Eng.*, Vol. 21, No. 6, pp. 503–505.

Zhang, Y., Zeng, H., Zhou, J., Xue, R., Sun, D. and Li, H., 2020. "Characterization of laser beam offset welding tini alloy and 304 stainless steel with different joining modes". *Optics & Laser Technology*, Vol. 131, p. 106372. ISSN 0030-3992. doi:https://doi.org/10.1016/j.optlastec.2020.106372. URL `https://www.sciencedirect.com/science/article/pii/S0030399220310057`.

6. RESPONSIBILITY NOTICE

The following text, properly adapted to the number of authors, must be included in the last section of the paper: The author(s) is (are) solely responsible for the printed material included in this paper.